Scripta Materialia 146 (2018) 213–217

Contents lists available at ScienceDirect

Scripta Materialia

journal homepage: www.elsevier.com/locate/scriptamat

Regular article

Dose rate dependence of Cr precipitation in an ion-irradiated Fe—18Cr alloy

Elaina R. Reese [a], Nathan Almirall [b], Takuya Yamamoto [b], Scott Tumey [c], G. Robert Odette [b], Emmanuelle A. Marquis [a,*]

[a] Department of Materials Science and Engineering, University of Michigan, Ann Arbor, MI 48109, USA
[b] Materials Department, University of California, Santa Barbara, CA 93106, USA
[c] Lawrence Livermore National Laboratory, Livermore, CA, 94550, USA

ARTICLE INFO

Article history:
Received 22 August 2017
Received in revised form 19 November 2017
Accepted 21 November 2017
Available online xxxx

Keywords:
Fe-Cr
Ion irradiation
Precipitation
Dose rate
Atom probe tomography

ABSTRACT

Precipitation of α′ in Fe—Cr alloys under neutron irradiation is thermodynamically driven while being accelerated by radiation-enhanced diffusion. However, similar alloys under ion irradiation at high dose rates ($>10^{-4}$ dpa/s) fail to exhibit α′ precipitation. Here, the microstructure of an Fe—18Cr alloy under ion or neutron-irradiation at 300 °C at dose rates from ~10^{-7} to 10^{-4} dpa/s was analyzed by atom probe tomography. The steady-state composition content of the clusters depends on the ion irradiation dose and dose rate, confirming the contribution of ballistic mixing in diluting the Cr concentration in non-equilibrium α′ precipitates.

Ferritic/martensitic (F/M) alloys, with high Cr content, are leading candidates for nuclear reactor components because of their corrosion resistance and favorable mechanical properties [1]. However, the evolution of F/M alloy microstructures and the corresponding degradation of their mechanical properties under neutron irradiation are a concern. One issue is the hardening and embrittlement caused by the precipitation of the α′ phase observed in both model and commercial Fe—Cr alloys under varying neutron irradiation conditions [2–8].

Prior observations of α′ precipitation in neutron-irradiated Fe—Cr alloys above 300 °C, are consistent with a thermodynamically driven process that is kinetically accelerated by radiation-enhanced diffusion (RED) [3,4,8–12]. Small angle neutron scattering (SANS) and atom probe tomography (APT) studies of neutron-irradiated and thermally aged model Fe—Cr alloys found near equilibrium α′ compositions, from 80 to 95 at.% Cr for temperature from 320 to 500 °C [6,12–15]. However, a number of APT studies on binary Fe—Cr alloys also reported significantly lower than equilibrium Cr concentrations, down to <50 at.% Cr, generally for smaller α′ precipitates ($r < 1$ to 1.5 nm) [5,16]. These values were rationalized in terms of technique artifacts [12,17] including data analysis procedures [16], alloying effects [7], interface energy effects on the local non-equilibrium thermodynamics [13], and perhaps some contribution of ballistic mixing [12].

While the α′ phase is observed in ferritic alloys containing >9 at.% Cr and neutron-irradiated at 300 °C, self-ion irradiations of similar alloys in the temperature range of 300 to 500 °C and up to 400 dpa yielded no clustering at high dose rates (10^{-3} to 10^{-2} dpa/s) [18,19]. At lower dose rates (10^{-5} to 10^{-4} dpa/s), limited clustering [20], in addition to dilution and dissolution of precipitates or spinodal structures [21,22] were observed. In contrast, electron irradiations at ~300 °C at intermediate dose rate of 4×10^{-5} dpa/s produced distinct α′ precipitates with the near equilibrium Cr concentration (96 at.% Cr) [23,24]. Proton irradiation of a commercial HT9 alloy at 400 °C to 7 dpa at 10^{-5} dpa/s, yielded distinct α′ precipitates, but with a low non-equilibrium Cr concentration (48 at.%) [25], that cannot be fully explained by the technique and analysis limitations described above. Instead, the modification or suppression of α′ precipitation need to be analyzed in light of differences among the neutron, ion, electron, and proton irradiation conditions.

Ballistic dissolution plays a less significant role in proton irradiations and much less in electron irradiations than in neutron irradiations. These differences are in part related to the primary knock-on energies that are on average 35 keV, 5 keV, 200 eV and 60 eV in Fe for 1 MeV neutrons, self-ions, protons and electrons, respectively [26]. Another key difference is the much higher dose rates at which ion irradiations are typically conducted. Therefore, the most important mechanism is the increase in interstitial and vacancy recombination with dose rate, since RED of Cr that leads to accelerated α′ precipitation depends on the defects that escape recombination or annihilation at irradiation-induced sinks. It is

* Corresponding author.
E-mail address: emarq@umich.edu (E.A. Marquis).

https://doi.org/10.1016/j.scriptamat.2017.11.040
1359-6462/

well established that higher dose rates delay precipitation to higher doses [27–31]; however, at sufficiently high dose, the precipitation of Cr would still saturate as the α matrix and α′ precipitates approach their respective phase boundaries. Another dose rate-dependent mechanism is related to the rate of ballistic mixing versus the rate of self-healing recovery that drives precipitates towards their equilibrium composition by thermal back diffusion of Cr. There is insufficient time for full recovery at high dose rates, while at low dose rates, self-healing is dominant. This mechanism qualitatively rationalizes the differences in α′ precipitation between proton [25], ion [20], and electron [23] irradiations performed at comparable dose rates.

To test the hypothesis that α′ precipitation is affected by dose rate, primarily by the ballistic mixing mechanism, a series of Fe self-ion irradiations were performed, spanning three orders of magnitude in dose rate. The resulting spatial distributions of Cr were quantified using APT. The ion irradiation results were also compared to lower dose rate neutron irradiations at 320 °C.

The Fe-18 at.% Cr alloy in this study has been included in several irradiation experiments dating back to the 1980s. Details of the solution annealing heat treatment used to produce a low dislocation density are summarized in [32]. Note that this alloy contained <0.1 at.% Si, V, and P and very few and isolated Si and P atoms clusters were observed (see Supplementary Material), but are not the focus of this work. The measured C contents was below 0.008 at.% with no noticeable contamination during irradiation. Two irradiations were performed at the Center for Accelerator Mass Spectrometry (CAMS) at Lawrence Livermore National Laboratory using a defocused beam of 70 MeV Fe^{2+} ions at 290 ± 5 °C. The same nominal doses (3 dpa at the damage peak) were reached at peak dose rates designed to be a factor of 10 apart. The dose profiles (Fig. 1) were estimated using SRIM calculations performed using the Kinchin-Pease model with a displacement energy of 40 eV [33]. The large penetration depth (~6 μm) of the 70 MeV ions allows examination of the effects of a correspondingly large range of dose and dose rates at various depths. To extend the range of dose, an additional 300 ± 5 °C ion irradiation was performed at the Michigan Ion Beam Laboratory (MIBL) using a defocused beam of 5 MeV Fe^{2+} ions to a nominal dose of 6.0 dpa at a depth of 0.5 μm and a dose rate of 3×10^{-5} dpa/s. Note the dose rates are based on estimates at the FIB liftout sample location. The MIBL experimental procedure is described elsewhere, e.g [34]. In addition, previously reported neutron irradiation data at 320 °C to ≈1.8 dpa [6] and 6.5 dpa [12] at a rate of 3×10^{-7} dpa/s was compared to the ion irradiation results.

APT specimens were prepared by following standard liftout and milling procedures using a FEI Helios 650 Nanolab scanning electron microscope (SEM) and focused ion beam (FIB) instrument. The apexes of the APT needles were positioned at various specified distances from the sample surfaces. The same depths were used for the two CAMS samples to compare the irradiation microstructures at the same dose. For the MIBL irradiation, APT specimens were extracted at depths between 0.5 and 0.6 μm to mitigate possible surface and/or end-of-range effects. Data collection was performed using a Cameca LEAP 4000XHR instrument operated in voltage pulsing mode using a pulse fraction of 20%, a pulse repetition rate of 200 kHz, data collection rate of 3 atoms per 1000 pulses, and specimen temperature of 50 K. The CAMECA Integrated Visualization & Analysis Software (IVAS) version 3.6.10 was used for data reconstruction. The values of the image compression factor and field factor were adjusted to the appropriate d-spacing between planes in visible and identifiable poles, and uniform depth and radial atomic densities [35]. The values of the image compression factor and field factor ranged between 1.2 and 1.5 and between 3.8 and 4.6, respectively.

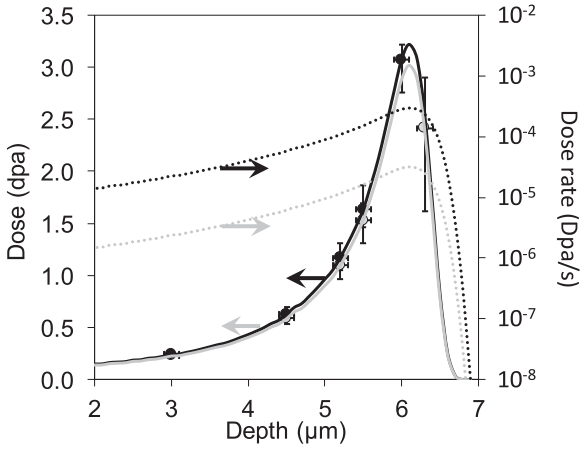

Fig. 1. Damage and dose rate profiles for the two CAMS irradiations.

Cr-rich regions, hereafter referred to as Cr clusters, were visible in all of the irradiation conditions, with characteristics that varied with dose and dose rates. Fig. 2 qualitatively highlights the differences in the spatial distribution of Cr atoms that are colored based on the local Cr concentration measured in spheres of 1 nm diameter. For a specified dose rate of ~10^{-5} dpa/s, the extent of Cr clustering visually increased with dose. Similarly, for a given dose (1.5 to 2 dpa), Cr clustering decreased with increasing dose rates. Among the ion-irradiated microstructures, the most significant clustering was observed for the doses of 2.4 and 6.0 dpa and dose rate of 3×10^{-5} dpa/s. In this case, the largest clusters reached a nominal core concentration of 55 ± 6 at. % Cr, that was estimated using a proximity histogram with a 28 at.% Cr isoconcentration surface and considering only the largest clusters with >1 nm radii. While this relatively low concentration value agrees with both prior ion- and neutron-irradiated data, e.g. [5,16, 19,22], it deviates significantly from the 320 °C neutron-irradiated data at 6.5 dpa and 3×10^{-7} dpa/s, where the composition of the larger Cr-rich clusters reached 84.2 ± 1.1 at. % [12].

The qualitative trends are clear. However, in the absence of well formed α′ precipitates, composition and size quantification of dilute clusters is difficult to determine from APT data. Thus, the amplitude of the Cr fluctuations and a size metric of the Cr-rich clusters for each irradiation condition were assessed using the radial distribution functions of the Cr atoms [36]. The curves were fitted using the equation suggested in [37]:

$$\frac{C_{Cr}(r)}{C^o_{Cr}} = \frac{A^2}{2{C^o_{Cr}}^2}\, cos\left(\frac{2\pi r}{\lambda_1}\right) exp\left(-\frac{r}{\lambda_2}\right) + 1$$

where $C_{Cr}(r)$ is the average concentration at the distance r from a Cr atom, C^o_{Cr} is the average matrix Cr concentration, $\frac{A^2}{2{C^o_{Cr}}^2}$ is the amplitude of the concentration fluctuations around the average C^o_{Cr}, λ_1 is the wavelength of the fluctuation, and λ_2 is the decay length of the fluctuation. The amplitude of the Cr fluctuations, which does not bear a one to one relation to the discrete core concentration, but rather reflects a quantified trend in how discrete Cr cluster compositions varied with the irradiation conditions (Fig. 3a). Notably, the amplitudes of the ion-irradiated clusters were significantly lower than those measured in the neutron-irradiated case. This reflects the much lower Cr concentrations in the ion-irradiated clusters compared to those observed in the neutron-irradiated condition. The amplitudes appeared to saturate with increasing dose. Further, the decay length appeared to be a good approximation of cluster radius (Fig. 3b). For example, it was in very good agreement with previously measured cluster radii for 1.8 dpa neutron data [6]. For a given dose (2 ± 1 dpa), the amplitude ($\frac{A^2}{2{C^o_{Cr}}^2}$) and cluster size ($\lambda_2$) decreased with increasing dose rate, while the number density, represented as λ_1^{-3} increased (Fig. 3b). We note that the clusters were slightly smaller after ion irradiation and much larger in the Tissot et al.'s electron irradiation data [23], compared to the neutron irradiated conditions [6,12].